

# Weierstraß-Institut für Angewandte Analysis und Stochastik

im Forschungsverbund Berlin e.V.

Preprint

ISSN 0946 – 8633

## On a mathematical model for laser-induced thermotherapy

Antonio Fasano<sup>1</sup>, Dietmar Hömberg<sup>2</sup>, Dmitri Naumov<sup>3</sup>

submitted: November 3, 2008

<sup>1</sup> Università degli Studi di Firenze  
Dipartimento di Matematica “Ulisse Dini”  
Viale Morgagni 67/A  
50134 Firenze  
Italy  
E-Mail: fasano@math.unifi.it

<sup>2</sup> Weierstrass Institute  
for Applied Analysis  
and Stochastics  
Mohrenstr. 39  
10117 Berlin  
Germany  
E-Mail: hoemberg@wias-berlin.de

<sup>3</sup> Technische Universität Berlin  
Fakultät II  
Institut für Mathematik, MA 3-2  
Str. des 17. Juni 136  
10623 Berlin  
Germany  
E-Mail: naumov@math.tu-berlin.de

No. 1368  
Berlin 2008



---

2000 *Mathematics Subject Classification.* 92C50, 76Z05, 35Q80.

*Key words and phrases.* Laser treatment, cancer therapy, coagulation, bio-heat equation.

Edited by  
Weierstraß-Institut für Angewandte Analysis und Stochastik (WIAS)  
Mohrenstraße 39  
10117 Berlin  
Germany

Fax: + 49 30 2044975  
E-Mail: [preprint@wias-berlin.de](mailto:preprint@wias-berlin.de)  
World Wide Web: <http://www.wias-berlin.de/>

**ABSTRACT.** We study a mathematical model for laser-induced thermotherapy, a minimally invasive cancer treatment. The model consists of a diffusion approximation of the radiation transport equation coupled to a bio-heat equation and a model to describe the evolution of the coagulated zone. Special emphasis is laid on a refined model of the applicator device, accounting for the effect of coolant flow inside. Comparisons between experiment and simulations show that the model is able to predict the experimentally achieved temperatures reasonably well.

## 1. INTRODUCTION

Laser-induced thermotherapy (LITT) is a minimally invasive alternative to conventional cancer treatments. It is especially used for patients with liver metastases from colorectal primal tumours or breast cancer. A recent study suggests that LITT may offer greater benefit than surgery for patients with liver metastases [11], see also [1].

As depicted in Figure 1, a catheter is used to place an applicator device into the tumour. It consists of a glass fiber with a diffusing tip surrounded by a coolant. The applicator is connected to a laser source. The fraction of the laser light which is absorbed by the tissue leads to a rise in temperature. The laser power and treatment time are adjusted such that a temperature of around  $60\text{ }^{\circ}\text{C}$  is reached in a neighbourhood of the applicator. Thereby, the tissue is coagulated, a process which is governed by protein denaturation leading to the disrapture of cell walls and eventually to the destruction of the tumour tissue. The deadened tissue remains in the body and is either decomposed or encapsulated.

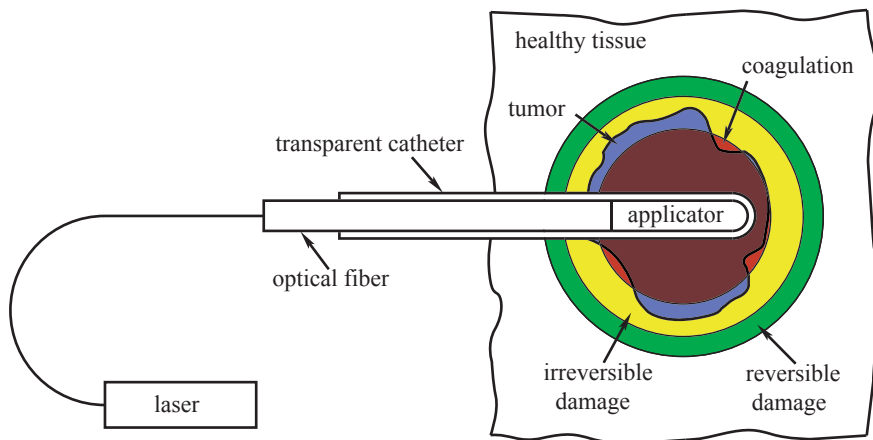


FIGURE 1. Sketch of laser-induced thermotherapy.

The treatment is guided using magnetic resonance imaging (MRI). Unfortunately, MRI is known to have either a good spatial or a good temporal resolution, making it difficult to predict the final size of the coagulated zone. Hence, there is a strong demand for computer simulations of LITT to support therapy planning and finding an optimal dosage.

For our purpose, the description of the device summarized in Figure 1 is sufficient. More details can be found in [7, 10]. The main components of the mathematical model are a radiation transport equation coupled to the bio-heat equation and an equation describing the coagulated zone. In Section 2 we review the system of model equations. The particular contribution of this paper is a refined model of the applicator in Section 3, accounting especially for the influence of the coolant. Section 4 is devoted to numerical simulations and a comparison with experimental results.

## 2. THE MODEL

The laser radiation emitted through the applicator acts as a volumetric heat source in the tumour tissue. The optical properties of the tissue during the treatment depend on the evolving fraction of coagulated tissue. Radiation transport through the tissue can be described by the radiation transport equation [5]. However, since its numerical simulation is intricate and time consuming a number of simplified models have been developed. Here, we use the stationary diffusion approximation [8]

$$(1) \quad -\nabla \cdot (D(\zeta, x) \nabla \Phi) + \mu_a(\zeta, x) \Phi = 0.$$

Here,  $\Phi$  is the irradiance,  $\mu_a$  the absorption coefficient. Next, we introduce the scattering coefficient  $\mu_s$  and the anisotropy factor  $g$ , which ranges between 0.7 and 0.99 for most biological tissues (cf. [8]). Then the diffusion coefficient is given as

$$D(\zeta, x) = \left( 3 (\mu_a(\zeta, x) + \mu_s(\zeta, x) (1 - g(\zeta, x))) \right)^{-1}.$$

$\zeta$  measures the fraction of native tissue, i.e.,  $\zeta = 0$  means fully coagulated and  $\zeta = 1$  native tissue and we define

$$(2) \quad \begin{aligned} \mu_s(x, \zeta) &= \mu_{s,n}(x) + (1 - \zeta)(\mu_{s,c}(x) - \mu_{s,n}(x)), \\ \mu_a(x, \zeta) &= \mu_{a,n}(x) + (1 - \zeta)(\mu_{a,c}(x) - \mu_{a,n}(x)), \\ g(x, \zeta) &= g_n(x) + (1 - \zeta)(g_c(x) - g_n(x)), \end{aligned}$$

where the indices  $n$  and  $c$  denote the coefficients for the native and coagulated tissue, respectively. The applicator is not part of our computational domain  $\Omega$ . Let  $\Gamma_{appl}$  be the part of the boundary  $\partial\Omega$  through which radiation is emitted, then we obtain the following boundary condition for the irradiance:

$$(3) \quad -D(\zeta, x) \frac{\partial \Phi(x)}{\partial \nu} + \frac{1}{2} \Phi(x) = \frac{1}{|\Gamma_{appl}|} p, \quad \text{on } \Gamma_{appl}$$

$$(4) \quad -D(\zeta, x) \frac{\partial \Phi(x)}{\partial \nu} + \frac{1}{2} \Phi(x) = 0, \quad \text{on } \partial\Omega \setminus \Gamma_{appl},$$

where  $p$  denotes the power of the applied laser source and  $|\Gamma_{appl}|$  the measure of  $\Gamma_{appl}$ .

In laser medicine coagulation is defined as an optically visible irreversible cell destruction (necrosis) caused by the denaturation of proteins. Following [10], we use an Arrhenius formalism to model protein denaturation. To this end, we assume an initial distribution of native tissue to be given by  $\zeta(0, x) = \zeta_0(x)$ . In most cases it is equal to one, which means there is no coagulation of tissue present. However, in case of multiple treatments the distribution of native tissue can be non-uniform.

The coagulation process can be described by the ODE

$$\frac{\partial \zeta(t)}{\partial t} = -F(T(t)) \zeta(t),$$

where the right-hand side is given by

$$F(T(t)) := \begin{cases} 0 & \text{for } T < 44^\circ C, \\ A \exp\left(\frac{-G}{RT(t)}\right) & \text{else.} \end{cases}$$

with some positive coefficients  $A$  and  $G$  and the universal gas constant  $R$ . The two cases in the above equation are needed to prevent any (unrealistic) protein denaturation below  $44^\circ C$ . Values for  $A$  and  $G$  have to be identified for different kinds of tissue. The approximation

of the tissue coagulation process by only two parameters is very rough, since the tissue is consisting of several proteins. Therefore we generalize this approach to a heuristic model, where the coagulation status is a weighted sum of several coagulation states  $\zeta_i$  for different proteins. The weights  $c_i$  are representing the concentrations of different proteins:

$$\zeta(t) = \sum_{i=1}^N c_i \zeta_i(t), \quad \text{with} \quad \sum_{i=1}^N c_i = 1,$$

and the previous equations turn to

$$(5) \quad \frac{\partial \zeta_i(t)}{\partial t} = -F_i(T(t)) \zeta_i(t), \quad F_i(T(t)) := \begin{cases} 0 & \text{for } T < 44^\circ C, \\ A_i \exp\left(\frac{-G_i}{RT(t)}\right) & \text{else.} \end{cases}$$

The initial value has to be given for all proteins considered, i.e.,  $\zeta_i(0, x) = \zeta_{i,0}(x)$ .

The temperature distribution  $T(x, t)$  is governed by the bio-heat equation.

$$(6) \quad \rho(x, T) C_p(x) \frac{\partial T(x, t)}{\partial t} - \nabla \cdot (\kappa(x, T) \nabla T(x, t)) = Q(x, t, T),$$

where  $\rho$  is the density,  $c_p$  the specific heat capacity at constant pressure and  $\kappa$  the thermal conductivity. According to [10]  $c_p$  and  $\rho$  vary less than 1 % and  $\kappa$  not more than 5 % in the relevant temperature interval between  $37^\circ C$  and  $70^\circ C$ , say. Hence, they are assumed to be constant in the sequel.

The heat source term  $Q$  is a sum of absorbed laser radiation  $Q_L$  and the heat exchange due to blood perfusion and metabolic changes  $Q_B$ . The amount of absorbed laser radiation is given by the product of irradiance and absorption coefficient  $\mu_a$ , i.e.,

$$(7) \quad Q_L(x, t) = \mu_a(x, t) \Phi(x, t).$$

Neglecting metabolic changes, the term  $Q_B$  describes the heat exchange due to blood perfusion in the tissue. A change in the blood perfusion rate is one of the reactions to the thermal changes in the tissue. Different modelling approaches are dealing with effects of higher perfusion rates for temperatures between  $37$  and  $50^\circ C$  or effects of a thick vessel located near the applicator device.

In [6] a model with higher perfusion rates for the named temperature region is used resulting in a significant difference in the coagulated tissue volume. In [3] a more complicated model with different blood perfusion terms for different tissues (healthy and pathological) was used. In [7] a thick vessel near the applicator device and its effect on the coagulation volume is investigated. All these methods require knowledge about additional parameters. Instead we have chosen to apply the simple, but widely used Pennes ansatz [9] to account for the blood perfusion. It has been shown to be a good approximation at least if we can assume that in the domain of interest only capillary vessels are located. Moreover we have to assume an isotropic blood flow. Then the Pennes ansatz is given by

$$(8) \quad Q_B(x, t, T) = \nu_B(\zeta, x) \rho_B C_{p,B} (T_B - T(x, t)),$$

where  $\nu_B(\zeta, x) [cm^3 g^{-1} s^{-1}]$  is the perfusion rate,  $\rho_B$  is the density of the blood,  $C_{p,B}$  is the specific heat capacity of the blood, and  $T_B$  is the temperature of the arterial blood.

For the tumourous tissue we use the same model with different perfusion rates. It seems reasonable to assume lower blood perfusion rates in the tumour, because the vascular system is not as efficient as in the healthy tissue, due to its chaotic structure [10]. In the coagulated

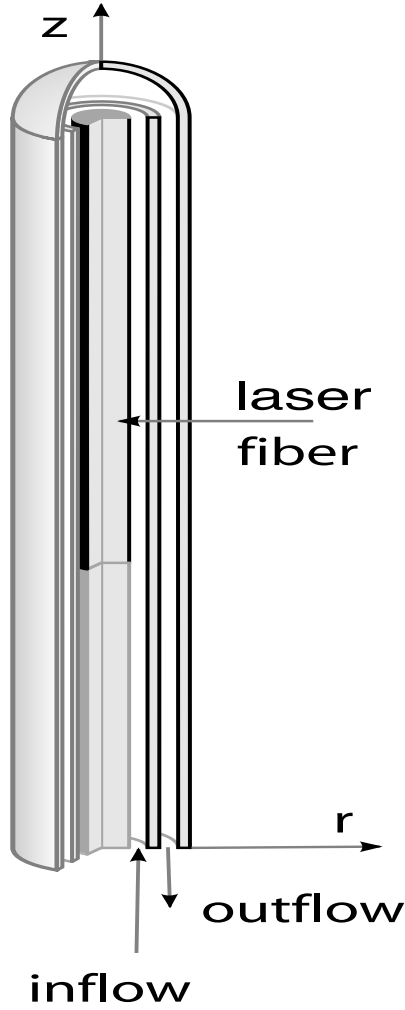


FIGURE 2. Schematic view of the applicator device.

tissue the vascular structure is destroyed and therefore the blood perfusion rate is zero in this region.

### 3. THERMAL ANALYSIS OF THE APPLICATOR

**3.1. The cooling device.** Figure 2 depicts a sketch of the applicator device. In cylindrical coordinates we denote  $\Gamma_{in} := [R_1, R_2]$  and  $\Gamma_{out} := [R_3, R_4]$  with  $0 < R_1 < R_2 < R_3 < R_4$  the inflow and outflow boundary, respectively.

The study of temperature distribution in the cooling device is effectively performed by means of rescaling. A suitable reference temperature is the difference  $\delta$  between the coagulation temperature  $\hat{T}_c$  and the normal body temperature  $T_{body}(\delta = 8^\circ C)$ .

Temperature  $\hat{T}$  is rescaled as  $T = \frac{\hat{T} - \hat{T}_{body}}{\hat{T}_c - \hat{T}_{body}}$ .

A typical length is the length of the applicator ( $L = 4cm$ ) (which is also comparable to the diameter of the coagulated region), and we rescale longitudinal coordinate  $\hat{z} \in (0, L)$  to  $z = \hat{z}/L$ .

For the moment we consider the coolant flow in a generic gap  $R_a < \hat{r} < R_b$ , and we denote by  $A$  the area of the gap cross section,  $A = \pi(R_b^2 - R_a^2)$ , and by  $v_0$  the average velocity of the flow

$$(9) \quad v_0 = \frac{1}{A} \int_{R_a}^{R_b} 2\pi\hat{r}\hat{v}(\hat{r})d\hat{r},$$

which we use to rescale velocity:  $v = \hat{v}/v_0$ . Note that by definition the average of  $v$  is equal to 1.

Since the leading phenomenon in the process is heat diffusion in the tissue, it is natural to rescale time by  $\tau_t = \frac{L^2\rho C}{\kappa}$ . Since the thermal properties of the tissue are similar to the ones of the coolant (water), defining for the latter the corresponding time  $\tau_c$ , we have  $\tau_t/\tau_c = O(1)$ . The rescaled time  $t$  is  $t = \hat{t}/\tau_t$ .

We also introduce the typical time of the advective flow  $\tau_a = \frac{L}{v_0}$ , so that the heat balance equation

$$(10) \quad \rho c \frac{\partial \hat{T}}{\partial \hat{t}} - k \left( \frac{\partial^2 \hat{T}}{\partial \hat{z}^2} + \Delta_r \hat{T} \right) + \rho c \hat{v}(\hat{r}) \frac{\partial \hat{T}}{\partial \hat{z}} = \mu \Phi,$$

takes the form

$$(11) \quad \frac{\partial T}{\partial t} - \frac{\tau_t}{\tau_c} \frac{\partial^2 T}{\partial z^2} - \frac{\tau_t}{\tau_c} L^2 \Delta_r T + \frac{\tau_t}{\tau_a} v \frac{\partial T}{\partial z} = \frac{\tau_t}{\rho c} \frac{1}{\hat{T}_c - \hat{T}_{body}} \mu_c \Phi_c.$$

The ratio  $\frac{\tau_t}{\tau_a}$  plays the role of a Peclet number  $Pe$ , since  $\tau_t \simeq 10^4$  s,  $\tau_a \simeq 10^{-1}$  s,  $Pe \simeq 10^5$ .

Dividing (11) throughout by  $Pe$ , we see that we can neglect the inertia term and that longitudinal diffusion is likewise negligible.

Next we observe that

$$(12) \quad \int_{R_a}^{R_b} 2\pi r k \Delta_r T = 2\pi k \left[ r \frac{\partial T}{\partial r} \right]_{R_a}^{R_b} = 2\pi [h_b R_b (T_{ext}^b - T^b) - h_a R_a (T_{ext}^a - T^a)],$$

where we have applied the boundary conditions

$$(13) \quad \begin{aligned} \kappa \frac{\partial T}{\partial r}(R_a, z) &= h_a (T_{ext}^a(z) - T(R_a, z)), \\ \kappa \frac{\partial T}{\partial r}(R_b, z) &= h_b (T_{ext}^b(z) - T(R_b, z)). \end{aligned}$$

We exploit the smallness of the ratio  $R_b/L$  to identify  $T(z, \hat{r}, t)$  with its average, which we still denote by  $T$ :

$$(14) \quad T(z, \hat{r}, t) \simeq T(z, t).$$

Moreover, we stress that the heat exchange condition taken at the boundary is justified in the presence of a thermal boundary layer (for  $v_0$  sufficiently large). The heat transfer coefficient depends on the thickness of the boundary layer, which in turn decreases when  $v_0$  increases. Therefore we write

$$(15) \quad h_a = \tilde{h}_a v_0, \quad h_b = \tilde{h}_b v_0,$$

where, within a certain range of  $v_0$ , the coefficients  $\tilde{h}_a, \tilde{h}_b$  (having the same dimensions as  $\rho_c$ ) depend on the device more than on the process.

If now we take the cross-sectional average of what survives in (11) with  $T = T(z, t)$ , exploiting the fact that the average of  $v$  is 1, we obtain

$$(16) \quad -\chi_b [T_{ext}^b - T - \frac{\tilde{h}_a R_a}{\tilde{h}_b R_b} (T_{ext}^a - T)] + \frac{\partial T}{\partial z} = \frac{L}{\rho c (\hat{T}_c - \hat{T}_{body}) v_0} \mu_c \Phi_c.$$

where

$$(17) \quad 2\pi \frac{\tau_a v_0}{\rho c A} \tilde{h}_b R_b = 2\pi \frac{L R_b}{\rho c A} \tilde{h}_b = \frac{L}{R_b} \frac{2\pi R_b^2}{A} \frac{\tilde{h}_b}{\rho c} := \chi_b.$$

For the specific experiment here examined we find  $\chi_b \simeq 0.067$  and in summary it can be concluded that in a typical situation ( $\frac{\partial T}{\partial z} \simeq 1.67$ ,  $T_{ext} - T \simeq 4 \cdot 1.67$ ) we have  $\chi_b (T_{ext} - T) / \frac{\partial T}{\partial z} \simeq 0.27$ , showing that the heat exchanged through each wall is of the same order as the heat convected longitudinally.

Equation (16) can be used for the temperature  $T_{in}$  of the inflowing coolant with the condition

$$(18) \quad T_{in}(0, t) = T_{in}^0$$

and  $R_a = R_1, R_b = R_2$ . In this case the temperatures  $T_{ext}^a, T_{ext}^b$  are the temperature  $T_g$  of the optical glass fiber and the temperature of the outflowing coolant  $T_{out}$ , respectively. The coefficients  $\tilde{h}_a, \tilde{h}_b$  refer to the corresponding boundaries. For the outflowing coolant equation (16) must be integrated backward with the condition

$$(19) \quad T_{ext}(1, t) = T_{in}(1, t)$$

and  $T_{ext}^a = T_{in}, T_{ext}^b = T_t$  (tissue),  $R_a = R_3, R_b = R_4$ .

**3.2. The glass fiber.** Using subscript  $g$  for the quantities referring to glass, introducing the approximation

$$(20) \quad T_g(z, \hat{r}, t) \simeq T_g(z, t)$$

and applying the same procedure of averaging over cross-sections, we obtain the equation

$$(21) \quad \frac{\partial T_g}{\partial t} - \frac{\tau_t}{\tau_g} \frac{\partial^2 T_g}{\partial z^2} + 2 \frac{h_g}{\rho_g c_g} \frac{\tau_t}{R_g} (T_g - T_{in}) = \frac{\tau_t}{\rho_g c_g (\hat{T}_c - \hat{T}_{body})} \mu_g \Phi_g.$$

The coefficient of  $(T_g - T_{in})$  can be given the form  $\frac{\tau_t}{\tau_a} \chi_g$  with  $\chi_g = 2 \frac{L}{R_g} \frac{\hat{h}_g}{\rho_g c_g}$ , and  $\hat{h}_g = h_g / v_0$ .

Since  $\chi_g$  is of the same order as  $\chi_b$ , it turns out that  $\frac{\tau_t}{\tau_a} \gg 1$ , which allows us to neglect the first two terms in (21).

Now we have two possibilities: either

(i) the same coefficient is much larger than the free term in (21), i.e.

$$(22) \quad 2 \frac{h_g}{R_g} \gg \mu_g \Phi_g \frac{1}{\hat{T}_c - \hat{T}_{body}}$$

then we deduce that

$$(23) \quad T_g \simeq T_{in},$$



or

(ii) the two sides of (22) are of the same order, then

$$(24) \quad \hat{T}_g - \hat{T}_{in} = \frac{R_g}{2\tilde{h}_g} \mu_g \Phi_g.$$

Of course the choice between (23) and (24) depends on the relative rates of thermal energy accumulation by the glass and thermal energy removed from the flow. In normal operating conditions (23) is the right option.

**3.3. Summary of the equations.** In the above we have neglected the thermal capacity of the glass walls of the device. Using (23) the equations describing the whole applicator are

$$(25) \quad \frac{\partial T_{in}}{\partial z} - \chi_2(T_{out} - T_{in}) = \frac{L}{\rho c v_0 (\hat{T}_c - \hat{T}_{body})} \mu_c \Phi_c$$

with  $\chi_2 = \frac{L}{R_2} \frac{2R_2^2}{R_2^2 - R_1^2} \frac{\tilde{h}_f}{\rho c}$ , where  $\tilde{h}_f$  refers to the heat exchange between the flow in and the flow out,

$$(26) \quad \frac{\partial T_{out}}{\partial z} - \chi_4 [T_t - T_{out} - \frac{\tilde{h}_f R_3}{\tilde{h}_t R_4} (T_{in} - T_{out})] = \frac{L}{\rho c v_0 (\hat{T}_c - \hat{T}_{body})} \mu_c \Phi_c$$

with  $\chi_4 = \frac{L}{R_4} \frac{2R_4^2}{R_4^2 - R_3^2} \frac{\tilde{h}_t}{\rho c}$ , and  $\tilde{h}_t$  referring to the heat exchange with the tissue.

The system is complemented by conditions (18), (19).

**3.4. Remarks on error sources.** Condition (19) eliminates the intermediation of the fluid in the tip region between the flow in and the flow out. The tip is characterized by the presence of stagnation. Clearly this procedure will lead to a relatively high error in the estimation of the temperature in and near the tip. However the volume of this region is so small that the main thermal field remains practically not affected.

Another source of error is having linearized the heat transfer of the applicator. Indeed, this tends to slightly underestimate the temperature close to the main body of the applicator. However, from the practical point of view such a discrepancy has no influence, since when the coagulation front has spread to the desired limit, some action has to be taken to coagulate the tissue close to the applicator, which has remained below the coagulation temperature during the whole process. What really matters is that the predicted temperature is in excellent agreement with the one measured over almost the whole coagulated mass, and in particular the prediction of the extension of the coagulated mass is quite accurate.

#### 4. NUMERICAL SIMULATIONS

To verify our model we consider ex-vivo experiments described by Roggan [10, p.145], in which pig liver has been exposed to a Nd:YAG laser with a cooled applicator as discussed in the preceding section. We consider two variants corresponding to a treatment with 20 W and 30 W, respectively. The exposure time in both cases was 10 min. For convenience, we have summarized all data used in the simulations in the appendix.

In Figures 3 and 4 the simulated temperature distribution at  $t = 600$  s is shown for  $P = 20$  W. A visual comparison to Roggan's experiment (Figure 5) shows, that there is not much of a

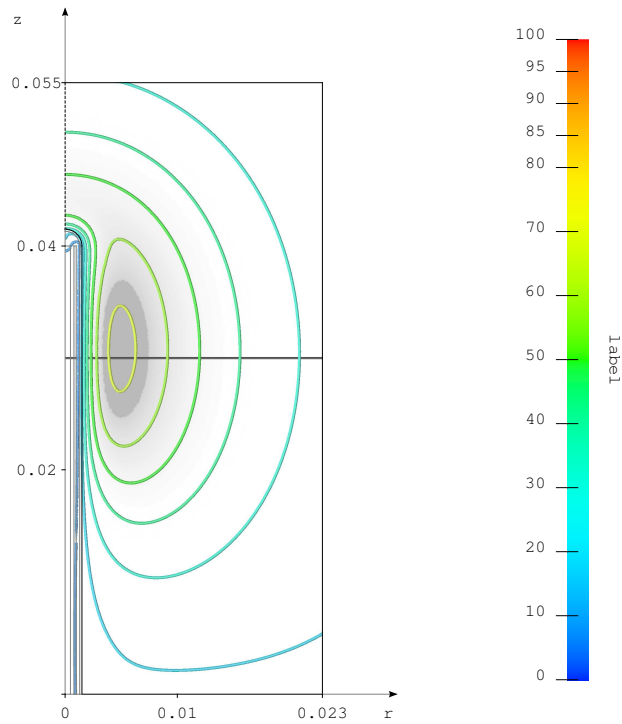


FIGURE 3. Temperature distribution and tissue coagulation at  $t = 600$  s of the simulation with  $P = 20$  W. The maximal temperature is  $80.6^\circ\text{C}$ . The greyly shaded area shows the coagulated tissue ( $\zeta_c \geq \zeta_b$ ). The line at  $z = 3$  cm indicates a cross-section line for the next figure.

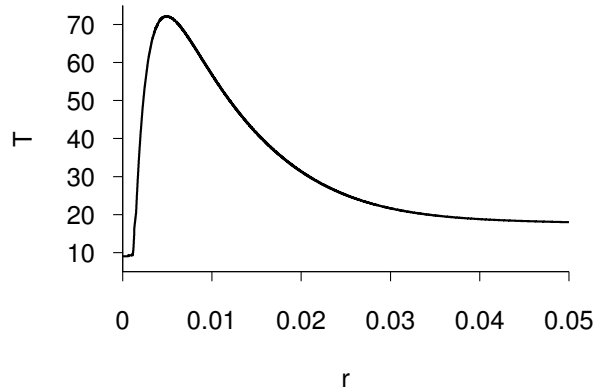


FIGURE 4. Cross-section plot of the temperature distribution of the simulation at  $z = 3$  cm corresponding to the previous figure.

difference in the distribution and maximal or minimal temperatures. The temperatures of the simulation slightly underestimate the temperatures of the experiment.

Unfortunately, there is no statement about the size of the coagulated zone for the 20W experiment in [10].

The second experiment corresponds to the higher laser power  $P = 30$  W. For this case, experimental results for the coagulated zone but not for the temperature distribution are reported.

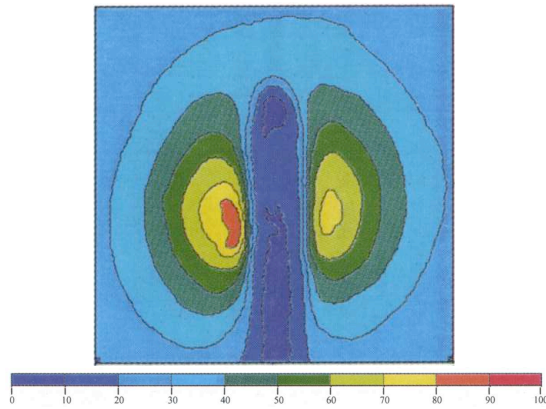


FIGURE 5. Temperature distribution at  $t = 600$  s of Roggan's experiment [10]. ( $P = 20$  W,  $T_{appl} = 9^\circ\text{C}$ ,  $T_{init} = T_{bnd} = 18^\circ\text{C}$ .)

Figure 6 shows the simulated temperature distribution and coagulated zone at  $t = 600$  s, i.e. at the end of the exposure time. For a better comparison between experimentally achieved coagulation zone and the simulated one, both are depicted in Figure 7. Both, experiment and simulation show a region of partly coagulated tissue. Moreover, although the core coagulated zone with complete necrosis seems to be slightly underestimated by the simulation, the region in which coagulation takes place at all is of merely the same size in experiment and simulation

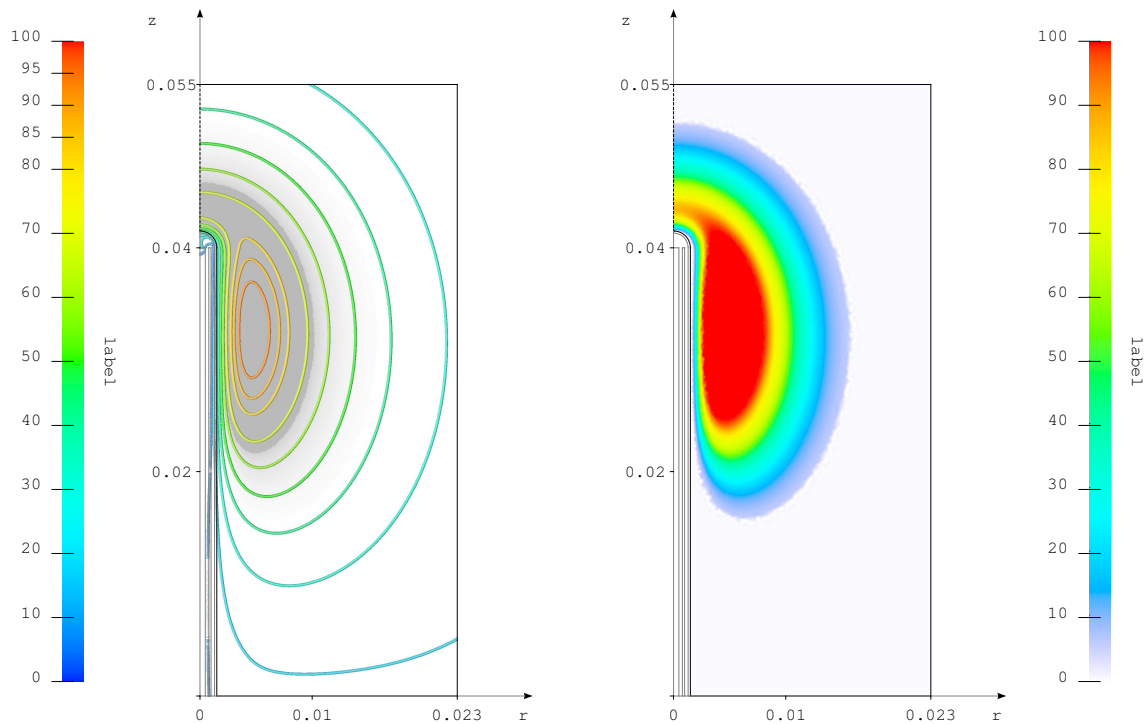


FIGURE 6. *Left*: Temperature distribution and tissue coagulation at  $t = 600$  s of the simulation with  $P = 30$  W. The maximal temperature is  $90.5^\circ\text{C}$ . The greyly shaded area shows the coagulated tissue ( $\zeta_c \geq \zeta_b$ ). *Right*: Tissue coagulation.

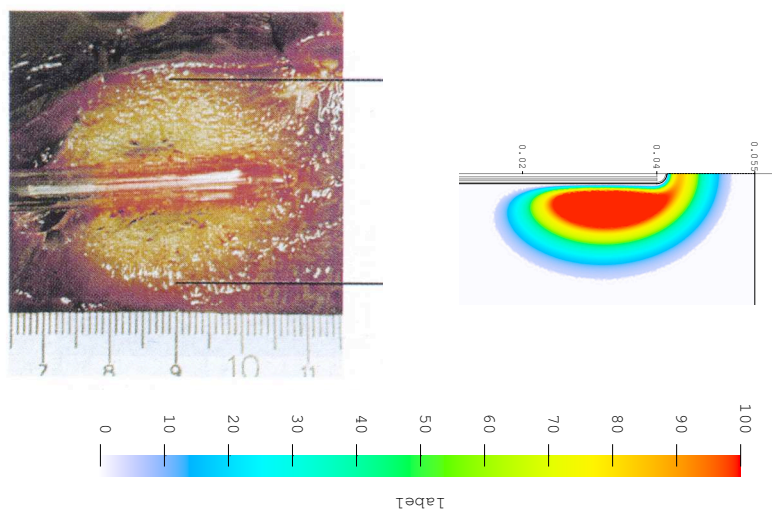


FIGURE 7. Distributions of coagulated tissue of Roggan’s experiment [10] (left) and simulation (right). ( $P = 30 \text{ W}$ ,  $T_{\text{appl}} = 9^\circ\text{C}$ ,  $T_{\text{init}} = T_{\text{bnd}} = 18^\circ\text{C}$ .)

## 5. CONCLUSIONS

We have investigated a mathematical model for laser-induced thermotherapy. The numerical results show that the model is capable of reproducing experimentally measured temperatures in the case of a cooled applicator. Hence, we may conclude that our approach to modelling the effect of the coolant is appropriate.

The numerical simulations underestimate the experimentally achieved coagulated zone. This is probably due to the fact that the simulation has been stopped at the end of the exposure time, since the experimental conditions after the treatments are not reported. In any case the coefficients in the damage model are fitting parameters which have to be chosen appropriately. From practical point of view it seems to be more promising to use phenomenological rate laws derived from Avrami-type models (see, e.g., [4]), which are frequently used to describe damage mechanisms in metals [2]. Then the temperature dependent coefficient can be computed as the solution of an inverse problem.

Another direction of future research is the study of related control problems to compute the optimal dosage as well as the optimal placement of the applicators, especially in the case, when more than one applicator is used.

## REFERENCES

- [1] F. Eickmeyer et al., *Survival after laser-induced interstitial thermotherapy of colorectal liver metastases – a comparison of first clinical experiences with current therapy results*. *Rofo*. **180** (2008), 35–41.
- [2] E. El-Magd, M. Brodmann, *Influence of precipitates on ductile fracture of aluminium alloy AA7075 at high strain rates*. *Mat. Science Eng. A* **307** (2001), 143–150.
- [3] B. Erdmann, J. Lang, M. Seebass, *Optimization of Temperature Distributions for Regional Hyperthermia Based on a Nonlinear Heat Transfer Model*. In: *Biotransport: Heat and Mass Transfer in Living Systems*, New York Academy of Sciences (1998), 36–46.
- [4] A. Fasano, *Mathematical models in polymer processing*. *MECCANICA J.* **35** (2000), 163–198.
- [5] Ishimaru, A., *Waves Propagation and Scattering in Random Media, Vol. I*, Academic Press, New York, 1978.

- [6] B.-M. Kim, et al., *Nonlinear Finite-Element Analysis of the Role of Dynamic Changes in Blood Perfusion and Optical Properties in Laser Coagulation of Tissue*. IEEE journal of selected topics in quantum electronics, **2** (1996), 922–933.
- [7] Y. Mohammed, J.F. Verhey, *A finite element method model to simulate laser interstitial thermo therapy in anatomical inhomogeneous regions*. BioMedical Engineering OnLine **4**:2 (2005).
- [8] Niemz, M., *Laser-Tissue Interactions, Fundamentals and Applications*. Springer, Berlin, 2002.
- [9] H.H. Pennes, *Analysis of tissue and arterial blood temperatures in the resting human forearm*. J. Appl. Phys **1** (1948), 93–122.
- [10] A. Roggan, *Dosimetrie thermischer Laseranwendungen in der Medizin: Untersuchung der speziellen Gewebeeigenschaften und physikalisch-mathematische Modellbildung*. Fortschritte in der Lasermedizin, Vol. 16, Hüthig Jehle Rehm, Landsberg/Lech (1997).
- [11] T. J. Vogl et al., *Effect of laser-induced thermotherapy on liver metastases*. Expert Rev Anticancer Ther. **6** (2006), 769–774.

#### APPENDIX A. DATA USED IN THE SIMULATIONS

The following two tables list all the parameters used in the simulations in Section 4. The optical parameters of the coolant were taken as those of distilled water. The same parameters were chosen for the walls of applicator device. The thermal properties of the coolant are those of distilled water at  $T = T_{ac}$ . The thermal properties of the applicator walls and of the laser fiber are those of silica glass. While the latter data have been taken from the COMSOL MULTIPHYSICS 3.3 material library, all the other parameters have been taken from [10].

Domain description	Optical parameters			Thermal parameters		
	$\mu_a$ ( $\text{mm}^{-1}$ )	$\mu_s$ ( $\text{mm}^{-1}$ )	$g$	$\rho$ ( $\text{kg m}^{-3}$ )	$C_p$ ( $\text{J kg}^{-1} \text{K}^{-1}$ )	$\kappa$ ( $\text{W m}^{-1} \text{K}^{-1}$ )
<u>Appl. device</u>						
Laser fiber	–	–	–	2203	703	1.38
Walls	0.266	3.0	0.98	2203	703	1.38
Coolant	0.266	3.0	0.98	999.9	4200	0.586
<u>Liver tissue</u>						
Native	0.0195	4.35	0.931	1040	3640	0.518
Coagulated	0.013	30.59	0.9165	1040	3640	0.518
Blood	–	–	–	1060	3640	–

The following table lists tissue coagulation parameters of the heuristic model based on the Arrhenius formalism, taken again from [10].

Symbol	Units	$i = 1$	$i = 2$	$i = 3$	$i = 4$
$A_i$	$\text{s}^{-1}$	$9.51 \cdot 10^{48}$	$5.20 \cdot 10^{59}$	$1.38 \cdot 10^{33}$	$1.00 \cdot 10^{23}$
$G_i$	$\text{J K}^{-1} \text{mol}^{-1}$	330444	411481	221361	138348
$c_i$	–	0.372	0.328	0.247	0.053